iScience

Article

SaaS sRNA promotes the interfering effect of *Salmonella* on hepatic iron metabolism via modulating ferroportin 1

Graphical abstract

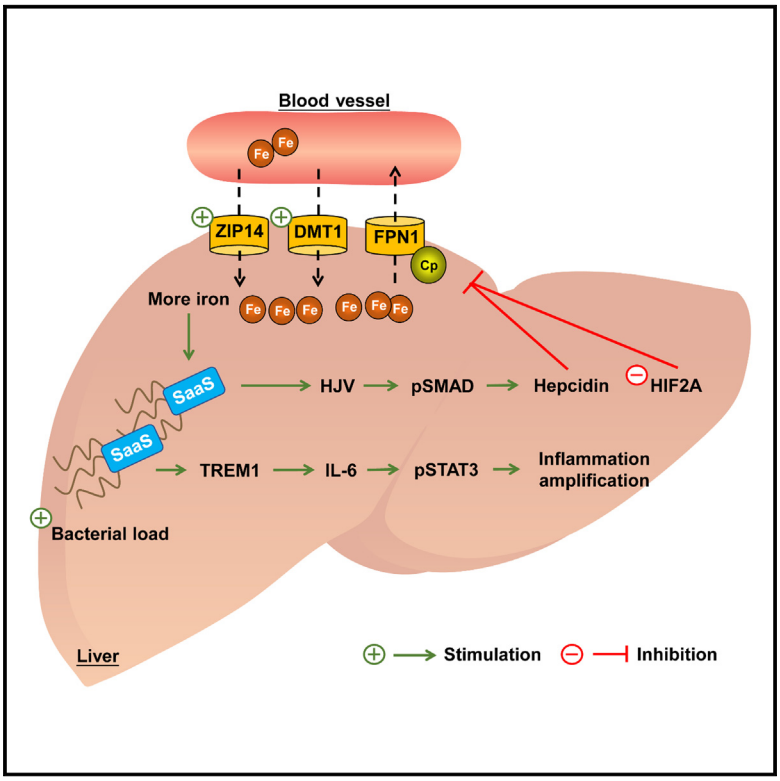

Authors

Linlin Cai, Yunting Xie, Haijing Hu, ..., Huhu Wang, Xinglian Xu, Guanghong Zhou

Correspondence

huuwang@njau.edu.cn (H.W.), xlxus@njau.edu.cn (X.X.)

In brief

Immunology; Microbiology

Highlights

- SaaS sRNA enhances the hepatic pathogenicity of *Salmonella*
- SaaS disturbs systemic iron metabolism by suppressing ferroportin 1
- SaaS activates the hepatic hepcidin-FPN1 axis by the *Hjv*-mediated BMP/SMAD pathway
- SaaS promotes hepatic inflammation by the TREM1-IL-6-mediated JAK/STAT3 pathway

Cai et al., 2025, iScience *28*, 111660
February 21, 2025
https://doi.org/10.1016/j.isci.2024.111660

CellPress

iScience

CellPress
OPEN ACCESS

Article

SaaS sRNA promotes the interfering effect of *Salmonella* on hepatic iron metabolism via modulating ferroportin 1

Linlin Cai,[1] Yunting Xie,[1] Haijing Hu,[1] Chongyang Lv,[1] Liangting Shao,[1] Huhu Wang,[1,2,3,*] Xinglian Xu,[1,*] and Guanghong Zhou[1]

[1]Key Laboratory of Meat Processing (Ministry of Agriculture), State Key Lab of Meat Quality Control and Cultured Meat Development (Ministry of Science and Technology), Jiangsu Collaborative Innovation Center of Meat Production and Processing, College of Food Science and Technology, Nanjing Agricultural University, Nanjing, Jiangsu 210095, P.R. China
[2]Xinjiang Agricultural University, Urumqi, Xinjiang 830052, P.R. China
[3]Lead contact
*Correspondence: huuwang@njau.edu.cn (H.W.), xlxus@njau.edu.cn (X.X.)
https://doi.org/10.1016/j.isci.2024.111660

SUMMARY

Iron limitation plays a fundamental role in host immunity against *Salmonella* infection. The mechanisms by which *Salmonella* antagonizes nutritional immunity, particularly those regulated by small non-coding RNAs (sRNAs), remain incompletely understood. In this study, we investigated the role of a previously identified sRNA, *Salmonella* adhesive-associated sRNA (SaaS), in host iron metabolism. Utilizing a combined BALB/c mouse model and HepG2 cell model, we demonstrated that SaaS enhances hepcidin synthesis via the bone morphogenetic protein (BMP)-SMAD pathway, leading to decreased ferroportin 1 level. This suppression of ferroportin 1 results in reduced serum iron and increased hepatic iron accumulation, ultimately causing iron-deficiency anemia. The accumulation of iron triggers hepatic oxidative stress, exacerbating liver damage. Concurrently, SaaS activates the signal transducer and activator of transcription 3 (STAT3) pathway in a triggering receptor expressed on myeloid cells-1 (TREM1)-interleukin (IL)-6-dependent manner, intensifying the inflammatory response. Collectively, these results provide evidence that sRNAs serve as crucial regulators of *Salmonella* pathogenesis and underscore the potential of targeting sRNAs for the prevention of salmonellosis.

INTRODUCTION

Non-typhoidal *Salmonella* (NTS) represents a significant public health challenge globally. Unlike typhoidal *Salmonella*, which causes the systemic disease of typhoid and is primarily confined to developing countries, NTS is found worldwide. NTS typically leads to self-limiting subacute or acute gastroenteritis, characterized by diarrhea, abdominal pain, and vomiting in individuals of all ages[1,2]; however, the dissemination of NTS throughout the body, including various extra-intestinal tissues such as the liver, can result in life-threatening septicemia.[3] This form of salmonellosis poses an ongoing risk and is one of the most considerable contributors to the high global burden of disease, particularly in Africa and Southeast Asia.[4] NTS comprises numerous serovars, with *Salmonella* Enteritidis being one of the most commonly implicated pathogens. *S*. Enteritidis is a facultative anaerobic, gram-negative, food-borne enteropathogen that belongs to the Enterobacteriaceae family, affecting both humans and animals. Recently, *S*. Enteritidis has been frequently reported in outbreaks of food-borne illnesses.[5,6] Therefore, monitoring *S*. Enteritidis and understanding its mechanisms of invasion are crucial for preventing microbial infections and their progression.

Iron is an essential component for nearly all living organisms and is the most abundant transition metal found in the human body.[7] In bacteria, iron serves as a catalyst in cellular enzymatic processes by facilitating redox reactions and plays a critical role in several vital life processes, including nitrogen fixation, central metabolism, and DNA replication.[8] Furthermore, it significantly influences the intracellular proliferation and survival of *Salmonella*.[9] To prevent pathogens from acquiring iron and thereby inhibiting their growth, host cells employ various defense strategies to sequester iron during infections, a phenomenon known as nutritional immunity.[7] The general strategy involves reducing intracellular Fe^{2+} concentrations through mechanisms such as (1) inhibiting extracellular Fe uptake, (2) promoting Fe^{3+} storage in ferritin, or (3) increasing cellular Fe^{2+} efflux.[10] In response to fluctuations in iron availability within a host environment, many pathogens have evolved diverse strategies to divert iron from their hosts into their own metabolic pathways. For instance, *Salmonella* has been reported to activate various elements to promote its own iron acquisition, including the siderophore enterobactin,[3] UMPylator YdiU,[11] and small non-coding RNAs (sRNAs) known as RyhB paralogs.[12] Recent findings suggest that these sRNAs act as post-transcriptional regulators, influencing

physiological processes. This intense competition for limited iron resources significantly impacts the establishment, progression, and outcome of infections.

sRNAs are generally untranslated and range in length from 50 to 500 nucleotides.[13] They are well known for their roles in sensing and responding to environmental changes, such as DsrA, which is involved in redox balance and oxidative stress,[14] and FimR2, which is associated with bacterial motility *in vitro*.[15] In contrast, the *in vivo* environment is more complex and diverse, where sRNAs are believed to fulfill their potential in host-pathogen interactions, promoting bacterial survival and enhancing pathogenesis. Competition for iron is a critical aspect of the host-pathogen interaction during *Salmonella* infection. The hepcidin (encoded by Hamp) and ferroportin 1 (FPN1; encoded by *Fpn1*) form an essential combination responsible for maintaining iron balance in the body. FPN1 is recognized as the sole iron exporter, while hepcidin, primarily secreted by hepatocytes, can degrade FPN1 by binding to it and initiating its internalization, thereby preventing iron efflux.[16,17] Recent research has shown that following *Salmonella* infection, mice exhibit increased hepcidin synthesis and decreased FPN1 levels, with these changes contributing to the growth of *Salmonella in vivo*.[18] However, whether and how sRNAs modulate the interaction between *Salmonella* and the host hepcidin-FPN1 axis, and thus interfere with host iron homeostasis, remains unknown.

Our earlier research identified a small RNA, *Salmonella* adhesive-associated sRNA (SaaS), which is highly conserved across various *Salmonella* species, including serovars Enteritidis, Typhimurium, Newport, Heidelberg, and Agona.[19] This conservation suggests that sRNA SaaS plays a significant role in *Salmonella* functionality. Further investigations revealed the diverse mechanisms by which SaaS influences *Salmonella* functions, including the regulation of biofilm formation, mortality, systemic inflammation, and intestinal dissemination in mice. Recently, SaaS was shown to enhance the hepatic pathogenicity of *Salmonella*, particularly by increasing their ability to colonize the liver[20]; however, the underlying mechanism remains unclear. Therefore, the objective of this study was to elucidate the specific role of SaaS in *Salmonella* hepatic pathogenicity and its function in systemic iron metabolism *in vivo*. Our findings offer potential sRNA-based prevention targets and strategies to combat *Salmonella* infection and contribute to the understanding of the regulatory network through which *Salmonella* interacts with the host.

RESULTS

sRNA SaaS interferes with host iron redistribution and liver injury

This study assessed whether the sRNA SaaS enhances the hepatic pathogenicity of *Salmonella*. Mice infected with the wild-type (WT) strain and the SaaS complement strain (Δ*saaS*/p*saaS*) exhibited similar changes throughout the study. WT-infected mice demonstrated a significantly higher release ($p < 0.05$) of aspartate aminotransferase (AST), alanine aminotransferase (ALT), and lactate dehydrogenase in the serum over time compared to those infected with the SaaS mutant strain (Δ*saaS*) (Figure 1A), indicating aggravated liver injury. Given the complex etiology, the AST/ALT ratio, which serves as a more reliable indicator of liver functional impairment due to various acute and chronic liver diseases, was subsequently employed to assess the extent of liver injury attributed to SaaS. The results indicated that AST, rather than ALT, was the primary altered factor, as evidenced by the increased AST/ALT ratio (greater than 1; Figure 1A), confirming significant hepatocyte damage caused by *S*. Enteritidis. Furthermore, a higher AST/ALT ratio in the WT group further corroborated that SaaS enhances *Salmonella* hepatic pathogenicity.

Considering the liver's critical role in iron homeostasis, the host iron distribution across each group was evaluated. In alignment with the previous findings, the WT group exhibited significantly decreased serum iron levels and a corresponding significant increase in hepatic iron levels ($p < 0.05$) compared to the Δ*saaS* group (Figure 1B). Consistently, Prussian blue-DAB staining demonstrated a greater presence and intensity of sepia in the WT group compared to the Δ*saaS* group at both time points (Figure 1C), indicating a higher accumulation of hepatic iron. These results demonstrate that the SaaS sRNA is crucial for bacterial pathogenicity in damaging liver cells and disrupting host iron distribution.

SaaS disturbs systemic iron metabolism and induces iron-deficiency anemia

Iron redistribution and sequestration during infection can lead to anemia,[21] and this study evaluated the symptoms associated with host iron redistribution. As shown in Figure 2A, the levels of red blood cells (RBCs), hemoglobin (HGB), and hematocrit (HCT) in the WT group were significantly lower ($p < 0.05$) than those in the Δ*saaS* and control groups. Meanwhile, the erythrocyte indices, including mean corpuscular volume (MCV), mean corpuscular hemoglobin (MCH), mean corpuscular hemoglobin concentration (MCHC), and the coefficient of variation of RBC distribution width (RDW-CV), exhibited corresponding changes. There was no significant difference in the levels of MCV, MCH, MCHC, and RDW-CV between the WT group and the Δ*saaS* group at 72 h post infection (hpi). However, at 120 hpi, the levels of MCV and MCH were significantly lower in the WT group compared to the control and Δ*saaS* groups; conversely, the levels of MCHC were significantly higher in the WT group than in the control and Δ*saaS* groups. The higher MCHC in the WT group, despite insufficient hemoglobin synthesis and decreased MCV and MCH, may be attributed to a compensatory increase. Additionally, there was no significant difference in the levels of RDW-CV between the WT and Δ*saaS* groups, ruling out the possibility of an abnormal RBC size distribution and further indicating a homogeneous microcytic anemia,[22] such as iron-deficiency anemia. The expression of haptoglobin (*Hp*) was also assessed (Figure 2B), revealing that the levels of *Hp* mRNA in the *Salmonella*-treated groups were significantly higher than those in the control group at both 72 and 120 hpi, thus excluding the possibility of hemolytic anemia.[23] Subsequently, serum iron parameters were analyzed to elucidate detailed symptoms. The concentrations of unsaturated iron-binding capacity (UIBC), total iron-binding capacity (TIBC), and transferrin saturation (Tf sat) were significantly lower ($p < 0.05$) in the WT group compared to the Δ*saaS* group during infection (Figure 2B). Furthermore, serum ferritin levels were significantly lower

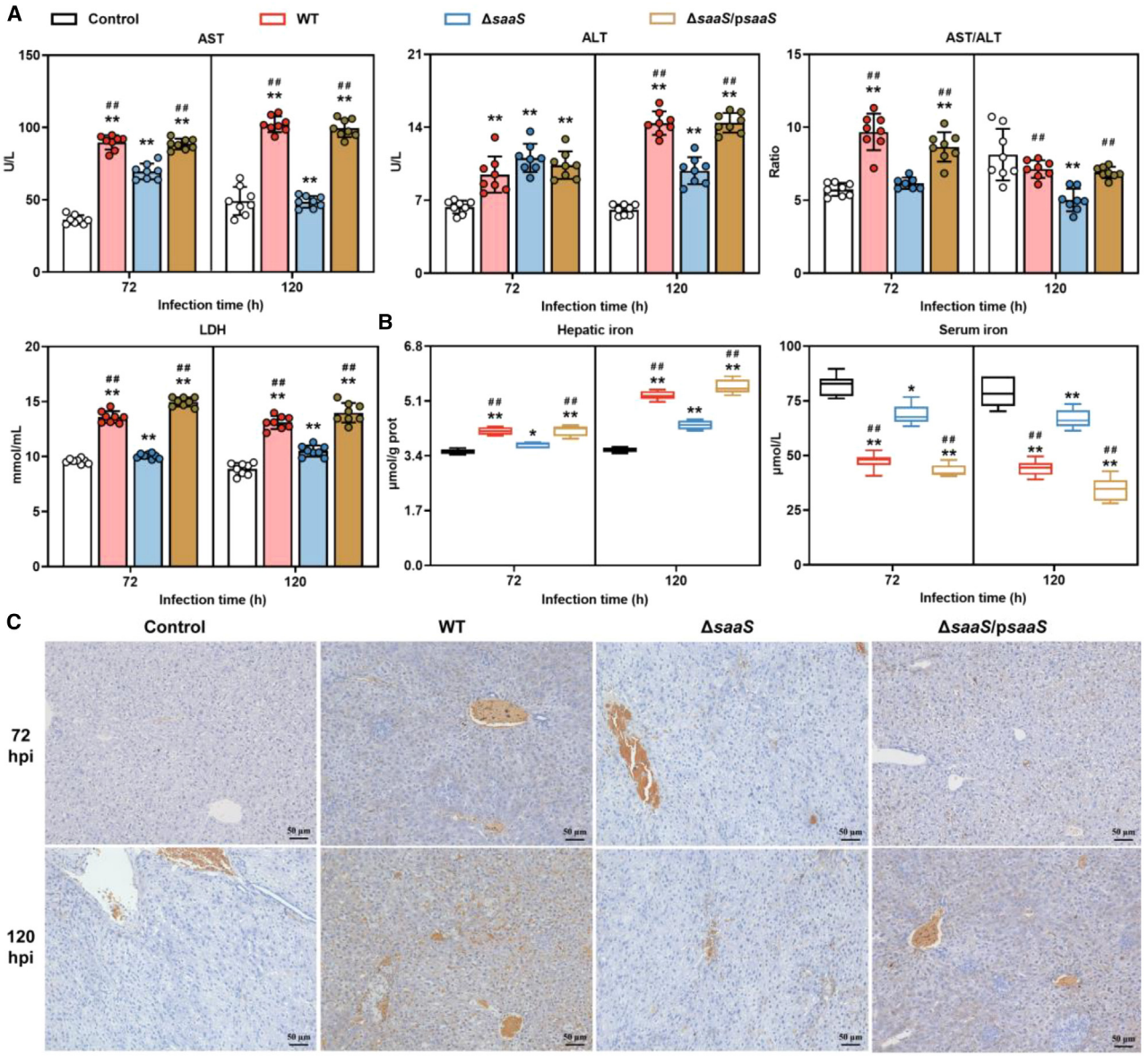

Figure 1. SaaS interferes with host iron redistribution and liver injury

(A) The concentration of serum aspartate aminotransferase (AST), alanine aminotransferase (ALT), and lactate dehydrogenase (LDH) and the ratio of AST to ALT after indicated infection length, $N = 8$.

(B) The concentration of hepatic and serum iron after indicated infection length, $N = 8$.

(C) Representative Prussian blue-DAB staining for iron in liver tissues after indicated infection length; original magnification, ×20 (scale bar, 50 μm).

Data are represented as mean ± SD. Statistical significance was determined by an independent Student's t test. $^{*}p < 0.05$, $^{**}p < 0.01$ versus control; $^{\#}p < 0.05$, $^{\#\#}p < 0.01$ versus Δ*saaS*.

($p < 0.05$) in the WT group than in the Δ*saaS* group during the later phase of infection (Figure 2C). Notably, serum ferritin levels were significantly higher in the WT group than in the Δ*saaS* group at 72 hpi. Our data demonstrate that SaaS-mediated *Salmonella* invasion disrupts systemic iron metabolism, resulting in systemic iron-deficiency anemia.

To evaluate potential relationships between bacterial burden and plasma and cellular iron status, Spearman's correlation analysis was conducted (Figure 2C). At 72 hpi, bacterial burden was positively correlated with hepatic iron and serum ferritin, while it was negatively correlated with serum iron, TIBC, and TF sat. Notably, with the exception of serum ferritin, these correlations were also observed at 120 hpi, where an additional seven correlations were identified: bacterial burden was positively correlated with RBCs, HGB, HCT, MCV, and MCH, while it was negatively correlated with MCHC and haptoglobin. This pattern indicates a worsening condition of iron-deficiency anemia during the SaaS-mediated *Salmonella* invasion.

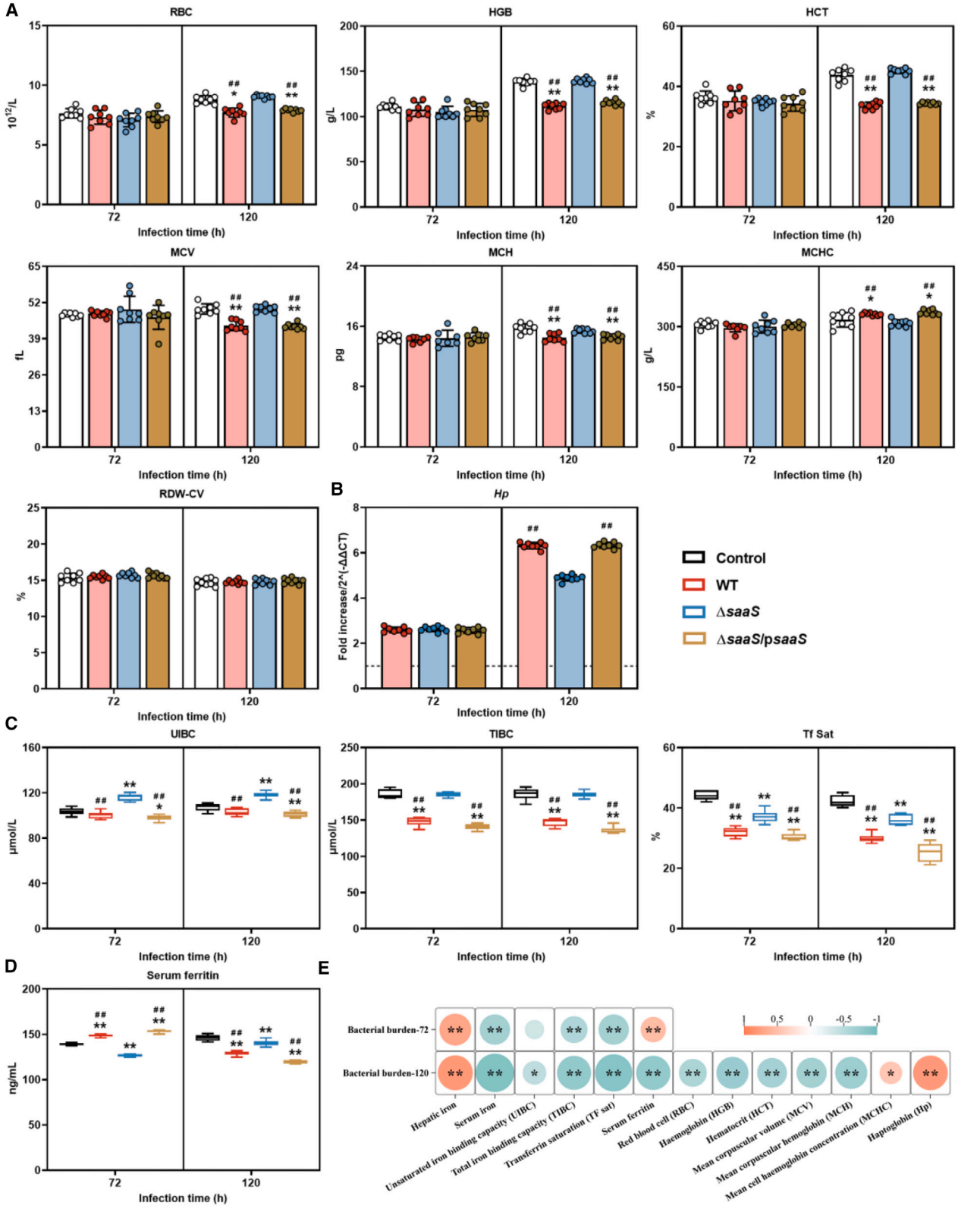

(legend on next page)

SaaS disturbs systemic iron metabolism by suppressing FPN1-mediated iron export

Maintaining the balance between iron export and uptake is vital for body iron homeostasis, with the hepcidin-FPN1 axis being a key regulator.[24] SaaS was hypothesized to contribute to *Salmonella*-induced systemic iron-deficiency anemia by affecting this axis. Analysis revealed that WT-infected mice had significantly lower hepatic FPN1 levels compared to the Δ*saaS* group at both time points, but significantly higher hepatic *Hamp* gene expression was only observed at 120 hpi in WT-infected mice (Figure 3A). This suggests that the successful activation of the hepatic hepcidin-FPN1 axis occurred during the late stage. Conversely, in the Δ*saaS* group, the expression of hepatic ceruloplasmin (encoded by *Cp*)—a protein involved in the binding of transferrin (TF; encoded by *Trf*) to iron and its transport in plasmawas approximately twice as high as that observed in the WT group. This finding indicates that SaaS plays a significant role in the widespread suppression of iron export during *Salmonella* invasion.

For iron uptake, we assessed the levels of critical genes in the TF route, including *Trf* and *Tfr1*, as well as in the non-TF route, which includes divalent metal transporter 1 (*Dmt1*) and zrt/irt-like protein 14 (*Zip14*) (Figures 3B and 3C). The expression of *Trf* and *Tfrc1* mRNAs was significantly lower ($p < 0.05$) in the WT group compared to the Δ*saaS* group, indicating that SaaS suppresses the TF route. In contrast, the expression of *Dmt1* and *Zip14* mRNAs was significantly higher in the WT group than in the Δ*saaS* group, demonstrating a pronounced time-dependent increase that suggests compensatory activation of non-TF iron uptake in response to the suppressed TF route. Therefore, we propose that by targeting FPN1, SaaS contributes to the suppression of iron export induced by *Salmonella*, leading to iron accumulation in the liver.

SaaS promotes the activation of the hepcidin-FPN1 axis through *Hjv*-mediated BMP/SMAD pathway

Hepatic hepcidin levels are primarily regulated by two independent signaling pathways: the bone morphogenetic protein (BMP)/SMAD pathway and the interleukin (IL)-6/Janus kinase (JAK)/signal transducer and activator of transcription 3 (STAT3) pathway.[25] To elucidate the signaling mechanism mediated by SaaS, we examined the protein phosphorylation levels of hepatic SMAD1/5/9 and STAT3 in mice infected with *Salmonella*. As illustrated in Figures 3D and 3E, the phosphorylation levels of SMAD1/5/9 and STAT3 in the WT-infected mice were significantly higher ($p < 0.05$) than those observed in the Δ*saaS*-infected mice.

We initially evaluated the BMP/SMAD pathway based on dramatic changes in pSMAD1/5/9 levels. Two distinct complexes were identified: one comprising matriptase-2 (TMPRSS6) and hemojuvelin (HJV), and the other consisting of the homeostatic iron regulator (HFE) and TFR2, both of which influence pSMAD levels independently of each other.[26,27] To investigate how SaaS facilitates the activation of the BMP/SMAD pathway, we assessed the expression levels of both complexes. As illustrated in Figure 4A, *Tmprss6* mRNA expression in the WT group was significantly lower than that in the Δ*saaS* group. In contrast, *Hjv* mRNA expression, which can be suppressed by *Tmprss6*, was significantly increased ($p < 0.05$) in the WT group compared to the Δ*saaS* group, indicating a potential activation of the TMPRSS6-HJV pathway. Importantly, no significant differences were observed in the levels of *Hfe* and *Tfr2* mRNAs throughout the study period, thereby excluding the regulatory involvement of the HFE and TFR2 complex.

To further elucidate the roles of *Tmprss6* and *Hjv* in SaaS-mediated *Salmonella* invasion, both genes were silenced using small interfering RNA (siRNA) in the HepG2 cell model. The efficacy of siRNA silencing in this study was confirmed by quantitative reverse-transcription PCR (RT-qPCR), achieving an efficiency greater than 70% (Figure S1). As illustrated in Figure 4B, during normal *Salmonella* invasion, the expression levels of *HAMP* and FPN1 levels in the WT group were significantly higher and lower, respectively ($p < 0.05$), compared to the Δ*saaS* group, aligning with the *in vivo* invasion results. Following transfection with *HJV* siRNA, no significant differences were observed in the expression levels of *HAMP* and FPN1 levels, indicating that HJV silencing could negate the effects of SaaS on hepcidin and FPN1 levels. Conversely, after transfection with *TMPRSS6* siRNA, significant differences ($p < 0.05$) in both *HAMP* and FPN1 levels between the WT group and the Δ*saaS* group persisted, showing no significant changes compared to those under negative control (NC) siRNA treatment. These results confirm that HJV, rather than TMPRSS6, is the critical regulatory site of the hepcidin-FPN1 axis mediated by SaaS.

SaaS contributes to the activation of the hepatic JAK/STAT3 pathway and promotes inflammatory response

To date, the IL-6-JAK/STAT3-estrogen receptor-related receptor γ (ERRγ)-mediated hepcidin synthesis pathway has been successfully established.[28] Recent studies have reported that

Figure 2. SaaS disturbs systemic iron metabolism and induces iron-deficiency anemia

(A) The levels of hematological parameters, including red blood cells (RBCs), hemoglobin (HGB), hematocrit (HCT), mean corpuscular volume (MCV), mean corpuscular hemoglobin (MCH), mean corpuscular hemoglobin concentration (MCHC), and the coefficient of variation of red blood cell distribution width (RDW-CV) after indicated infection length, $N = 8$.

(B) The expression of *Hp* mRNA (encoding haptoglobin) after indicated infection length, $N = 8$.

(C) The levels of serum iron parameters including unsaturated iron-binding capacity (UIBC), total iron-binding capacity (TIBC), and transferrin saturation (Tf sat) after indicated infection length, $N = 8$.

(D) The concentration of serum ferritin after indicated infection length, $N = 8$.

(E) The correlation analysis between the bacterial burden and plasma and cellular iron status; red color represents significant positive correlation, cyan color represents significant negative correlation, and the independent right color bars depict correlation coefficients.

Data are represented as mean ± SD. Statistical significance was determined by an independent Student's t test. $^{*}p < 0.05$, $^{**}p < 0.01$ versus control; $^{\#}p < 0.05$, $^{\#\#}p < 0.01$ versus Δ*saaS*.

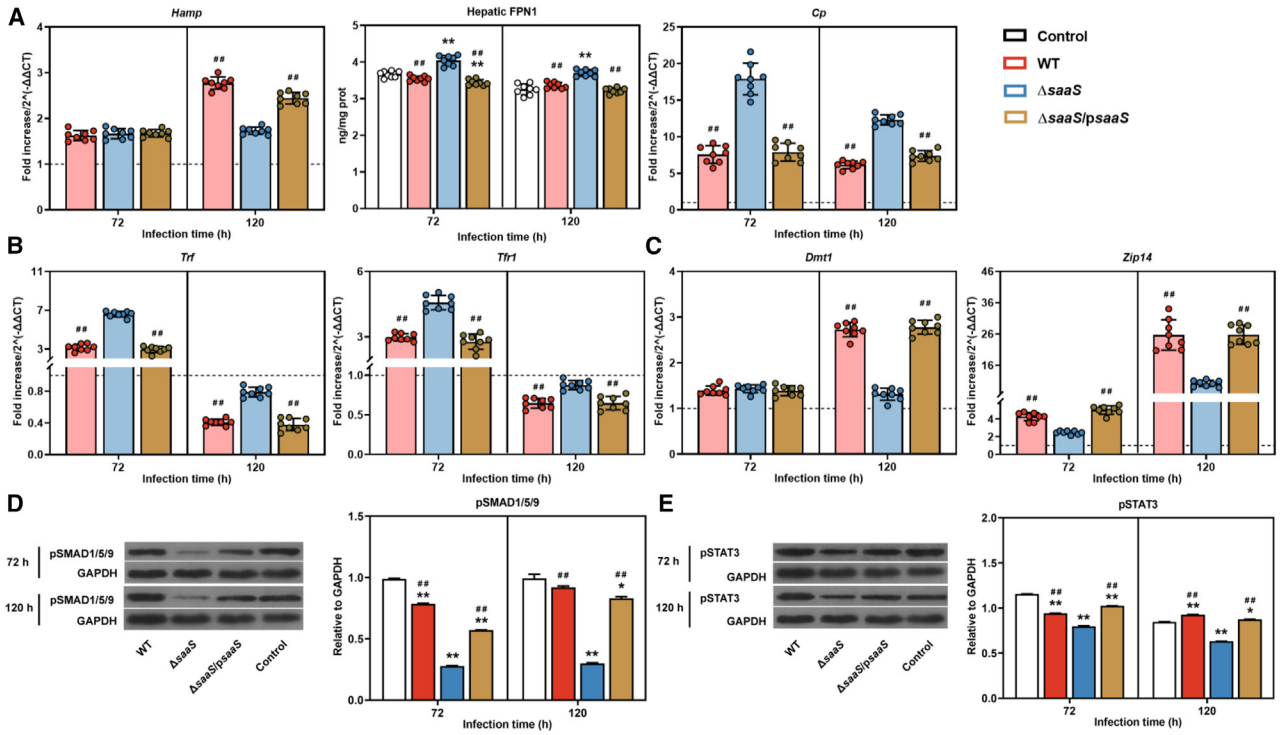

Figure 3. SaaS disturbs systemic iron metabolism by suppressing FPN1-mediated iron export

(A) The concentration of hepatic ferroportin 1 (FPN1) and the gene expression of *Hamp* (encoding hepcidin) and *Cp* (encoding ceruloplasmin) after indicated infection length, $N = 8$.

(B) The gene expression of hepatic transferrin pathway including *Trf* (encoding transferrin) and *Tfr1* (encoding transferrin receptor 1) after indicated infection length, $N = 8$.

(C) The gene expression of hepatic non-transferrin pathway including *Dmt1* (encoding divalent metal transporter 1) and *Zip14* (encoding zrt/irt-like protein 14) after indicated infection length, $N = 8$.

(D) Western blot analysis of liver lysates with specific antibodies to pSMAD1/5/9 after indicated infection length.

(E) Western blot analysis of liver lysates with specific antibodies to pSTAT3 after indicated infection length. For RT-qPCR analysis, the dash line was corresponding to the control group. For western blot analysis, densitometric analysis of both proteins to GAPDH protein is shown.

Data are represented as mean ± SD. Statistical significance was determined by an independent Student's t test. $^{*}p < 0.05$, $^{**}p < 0.01$ versus control; $^{\#}p < 0.05$, $^{\#\#}p < 0.01$ versus Δ*saaS*.

the triggering receptor expressed on myeloid cells-1 (TREM-1) promotes pro-inflammatory levels, particularly IL-6, which is implicated in hepcidin production.[18] To investigate the potential activation of this pathway, we evaluated the levels of IL-6 and the expression of *Trem1* and *Esrrg* (encoding ERRγ) mRNAs. As illustrated in Figure 5A, although the expression of *Trem1* mRNA and IL-6 levels was significantly higher ($p < 0.05$) in the WT group compared to the Δ*saaS* group during the later period, no significant difference was observed in the expression of *Esrrg* mRNA between the groups, indicating that hepcidin synthesis was not activated.

In addition to regulating hepcidin synthesis, the JAK/STAT pathway participates in a variety of biological processes, including apoptosis, inflammatory response, and immune regulation. Given the elevated IL-6 levels induced by SaaS, we inferred that the JAK/STAT pathway intensifies the inflammatory response in this study. As illustrated in Figure 5B, the levels of pro-inflammatory cytokines, including IL-1, tumor necrosis factor alpha, and interferon-γ, were significantly higher ($p < 0.05$) in the WT group compared to the Δ*saaS* group throughout the entire period. Although there was no significant difference in IL-10 levels between the groups, the levels of the anti-inflammatory cytokine transforming growth factor β were significantly lower ($p < 0.05$) in the WT group than in the Δ*saaS* group, indicating a clear pro-inflammatory effect of SaaS. These findings support our observation that SaaS activates STAT3 to promote the inflammatory response rather than hepcidin expression.

SaaS decreases hepatic FPN1 level by inhibiting *Hif2a* expression

In addition to the typical regulation of hepcidin, FPN1 is transcriptionally regulated by various transcription factors, including metal regulatory transcription factor 1 (*Mtf1*), the *Hif* family (*Hif1a* and *Hif2a*), and nuclear factor erythroid-2-related factor 2 (*Nrf2*).[29] Considering the decreased levels of FPN1 alongside undifferentiated hepcidin among the groups at the early stage, we determined the mRNA levels of *Hif1a*, *Hif2a*, *Mtf1*, and *Nrf2* to gain a comprehensive understanding of the downregulation of FPN1 mediated by SaaS. The expression of *Mtf1* and *Nrf2* mRNAs remained consistent across all groups throughout the

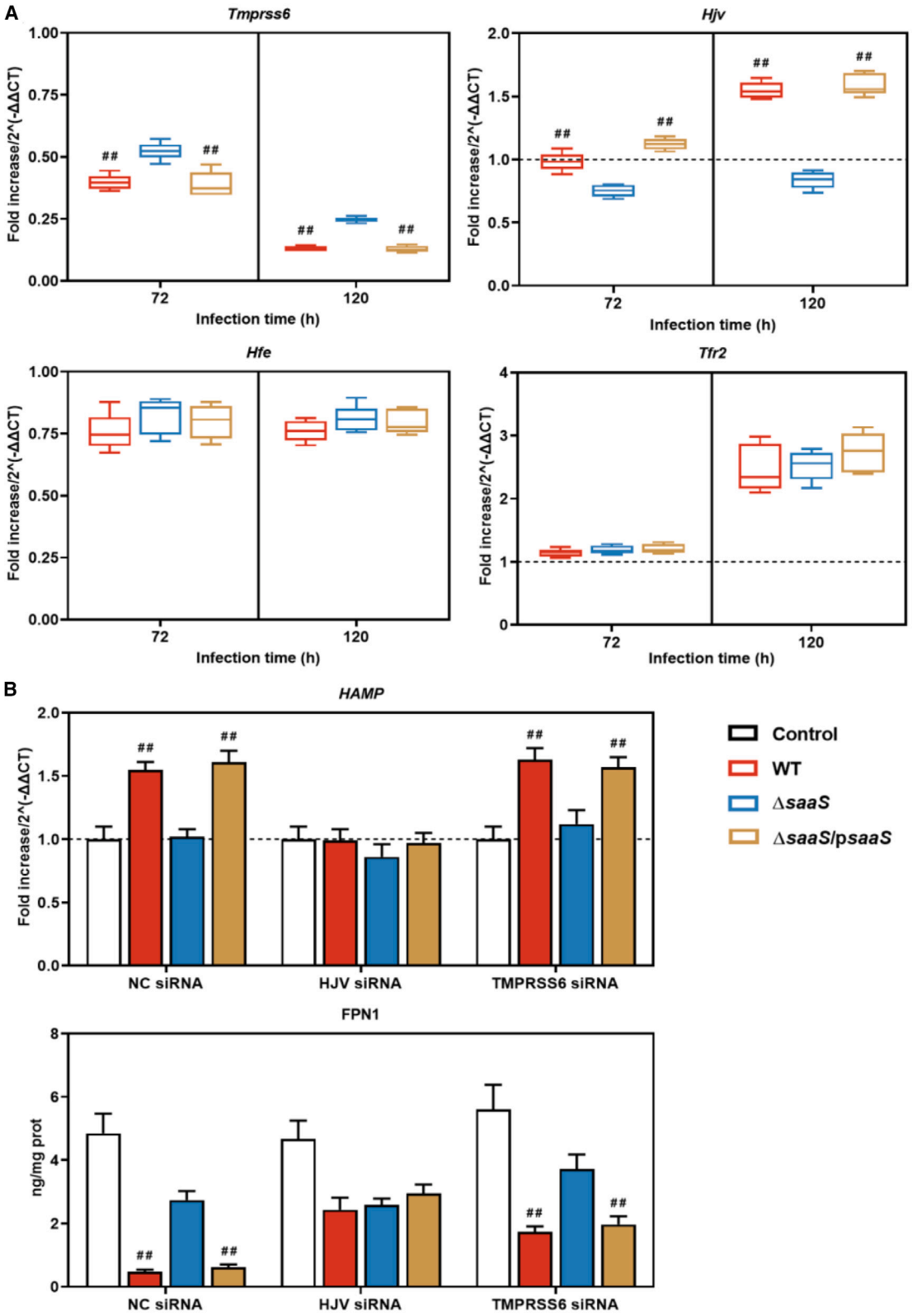

(legend on next page)

entire period (Figure 6A); however, the expression of the *Hif* family in the WT group was significantly lower ($p < 0.05$) compared to that in the Δ*saaS* group. Therefore, it was hypothesized that SaaS downregulates *Fpn1* mRNA levels through one or both members of the *Hif* family. To further investigate this, a HepG2 transfection and invasion model was established. Following transfection with *HIF1A* or *HIF2A* siRNA, significant differences ($p < 0.05$) in FPN1 levels between the WT group and the Δ*saaS* group persisted, with no notable changes observed compared to the NC siRNA treatment (Figure 6B). This indicates that SaaS does not utilize the *Hif* family to regulate FPN1 levels.

SaaS triggers oxidative stress but not ferroptosis in the liver

The accumulation of iron can lead to oxidative stress through the Fenton reaction. As illustrated in Figure 7A, the WT group exhibited significantly lower levels of catalase (CAT), superoxide dismutase (SOD), and glutathione (GSH), alongside significantly higher levels of malondialdehyde (MDA) compared to the Δ*saaS* group. These findings confirm that SaaS induces oxidative stress in the liver via iron accumulation.

Ferroptosis, a recently identified regulatory form of cell death, has garnered considerable attention.[30] Both iron overload and oxidative stress are known inducers of ferroptosis. Given the observed iron accumulation and the subsequent oxidative stress coupled with GSH downregulation, it is inferred that *Salmonella*, mediated by SaaS, induces host ferroptosis. As depicted in Figure 7B, although the expression of solute carrier family 11, member 1 (*Slc7a11*) mRNA was significantly lower ($p < 0.05$) in the WT group compared to the Δ*saaS* group, the protein levels of GPX4, a central regulator of ferroptosis closely associated with lipid peroxidation,[31] were significantly higher ($p < 0.05$) in the WT group throughout the entire infection period (Figure 7B). This suggests the presence of an active compensatory mechanism that prevents ferroptosis.

DISCUSSION

Both excessive and insufficient iron levels are detrimental, leading to tissue damage and resulting in conditions such as anemia or fibrosis. Given that the intracellular growth and replication of *Salmonella* require adequate iron, the restriction of iron is considered a critical component of the innate resistance to *Salmonella* infection, thereby protecting the host from severe symptoms.[10,18] Consequently, we hypothesized that *Salmonella* may utilize sRNAs to manipulate host iron availability. This study assessed the sRNA SaaS-mediated effects of *Salmonella* on the liver, a key organ involved in iron homeostasis. The results indicated that the increased hepatic bacterial burden due to SaaS resulted in more severe liver injury, characterized by decreased serum iron levels and increased hepatic iron content; multiple reports support this observation.[18,28] Serum iron limitation negatively impacts hemoglobin synthesis, leading to decreased HCT and anemia in iron-deficient states, with anemia being the most recognizable sign of iron deficiency.[32] Here, induced iron-deficiency anemia was confirmed by decreases in RBCs, HGB, HCT, and iron parameters such as UIBC, TIBC, and Tf sat, suggesting that the host was prompted to withhold iron from pathogens to inhibit their growth.[24] Consequently, this strategy resulted in hepatic iron retention. Notably, increased serum ferritin levels were observed only in the WT group at 72 hpi, a response also seen in mice infected with both *Salmonella* and *Listeria monocytogenes* at the same time point,[24] indicating a potentially common response during early infection.

Closely associated with infectious anemia, the hepcidin-FPN1 axis is a critical component of iron homeostasis and has been confirmed as a detrimental factor in host resistance to *Salmonella*, particularly by promoting hepatic bacterial loads.[18] As expected, the hepcidin-FPN1 axis was activated by SaaS, leading to hepatic iron accumulation and increased bacterial loads. The hepcidin-FPN1 axis has been reported to be exploited by intracellular pathogens to restrict the RBC pool in various organs and cells,[22,33] which partially explains the observed decrease in RBCs due to SaaS in this study. FPN1-associated iron efflux is typically coupled with the multi-copper ferroxidase CP,[34] and the depletion of either FPN1 or CP results in increased iron accumulation and heightened sensitivity of cells to ferroptosis.[35,36] Concurrently, along with decreased FPN1 levels, the expression of *Cp* mRNA was diminished by SaaS, leading to a reduced capacity for iron export. However, the effect of SaaS on hepatic iron absorption is complex, characterized by elevated non-TF iron uptake alongside a suppressed TF route. This suggests a compensatory activation of the host defense and underscores the specific role of SaaS in modulating iron export via the hepcidin-FPN1 axis. Therefore, further investigation is warranted to elucidate how SaaS achieves this modulation.

In contrast to the activation of the JAK/STAT3 pathway by the effector SpvB,[18] SaaS activated both the BMP/SMAD and JAK/STAT3 pathways, differentiating them by their distinct functions in this study. HJV is expressed in the liver, where hepcidin is produced. As a recently identified factor, HJV positively regulates the SMAD pathway and promotes the production of hepcidin, which is associated with tissue iron overload,[37] while TMPRSS6 can cleave membrane-bound HJV and negatively regulate hepcidin expression.[27] This work provides experimental evidence that during SaaS-mediated *Salmonella* infection, HJV is essential for positively regulating hepcidin expression and the subsequent expression of FPN1 in liver cells. In contrast, TMPRSS6 was found to be ineffective, partly due to its low expression levels. Similar to HJV in the BMP/SMAD pathway,

Figure 4. SaaS promotes the activation of the hepcidin-FPN1 axis through the Hjv-mediated BMP/SMAD pathway

(A) The gene expression of hepatic *Tmprss6* (encoding matriptase-2), *Hjv* (encoding hemojuvelin), *Hfe* (encoding homeostatic iron regulator), and *Tfr2* (encoding transferrin receptor 1) after indicated infection length, $N = 8$.

(B) The gene expression of *HAMP* (encoding hepcidin) and the concentration of ferroportin 1 (FPN1) in HepG2 cells infected with *Salmonella* after transfection with the corresponding small interfering RNA (siRNA), $n = 5$. For RT-qPCR analysis, the dash line was corresponding to the control group.

Data are represented as mean ± SD. Statistical significance was determined by an independent Student's t test. $^{*}p < 0.05$, $^{**}p < 0.01$ versus control; $^{\#}p < 0.05$, $^{\#\#}p < 0.01$ versus Δ*saaS*.

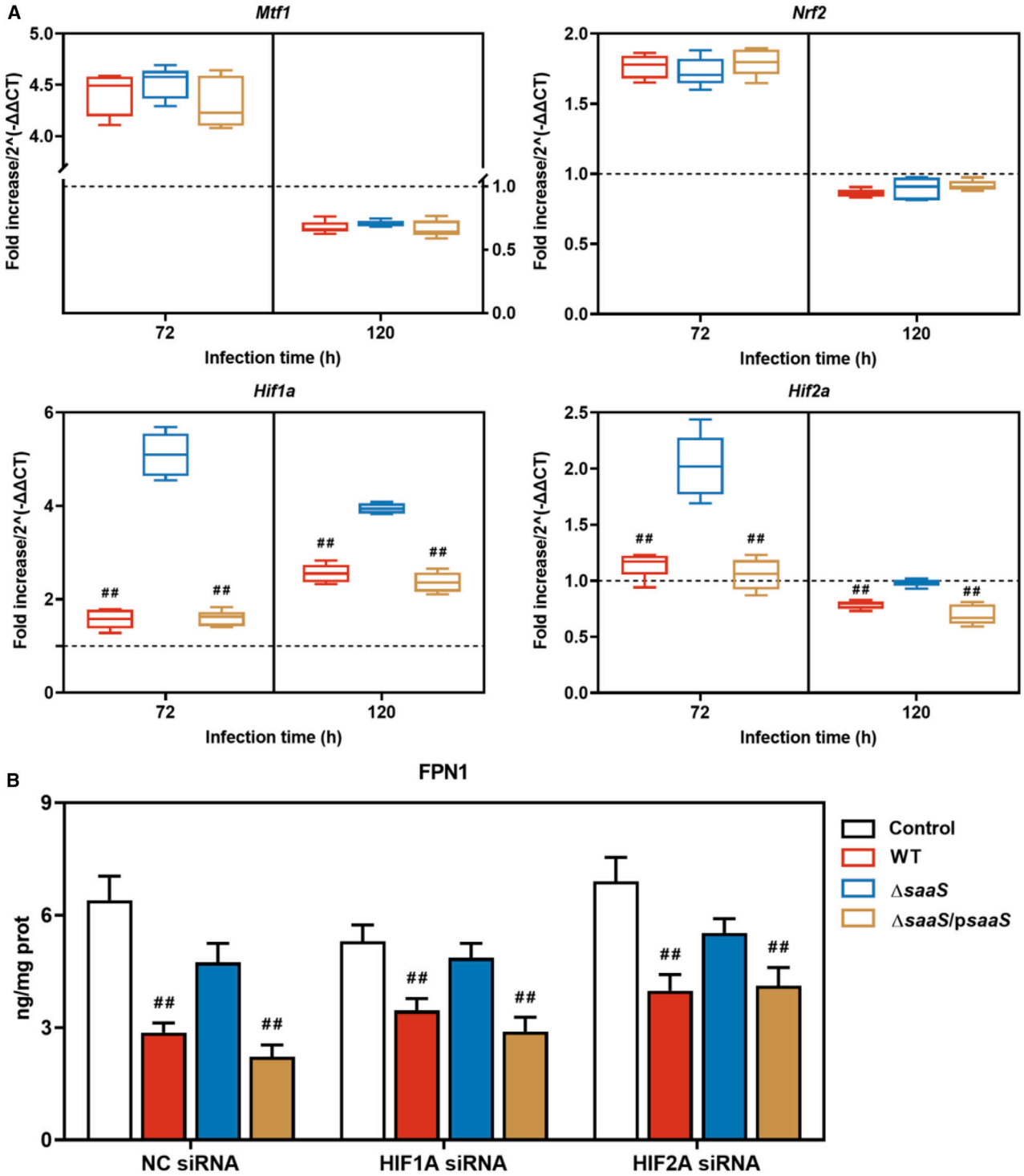

Figure 5. SaaS contributes to the activation of the hepatic JAK/STAT3 pathway and promotes inflammatory response

(A) The concentration of hepatic interleukin (IL)-6 and the gene expression of *Trem1* (encoding triggering receptor expressed on myeloid cells-1) and *Esrrg* (encoding estrogen receptor-related receptor γ) after indicated infection length, $N = 8$.

(B) The concentrations of inflammatory cytokines including interleukin (IL)-1β, tumor necrosis factor alpha (TNF-α), interferon-γ (IFN-γ), IL-10, and transforming growth factor β (TGF-β) after indicated infection length, $N = 8$. For RT-qPCR analysis, the dash line was corresponding to the control group.

Data are represented as mean ± SD. Statistical significance was determined by an independent Student's t test. $^{*}p < 0.05$, $^{**}p < 0.01$ versus control; $^{\#}p < 0.05$, $^{\#\#}p < 0.01$ versus Δ*saaS*.

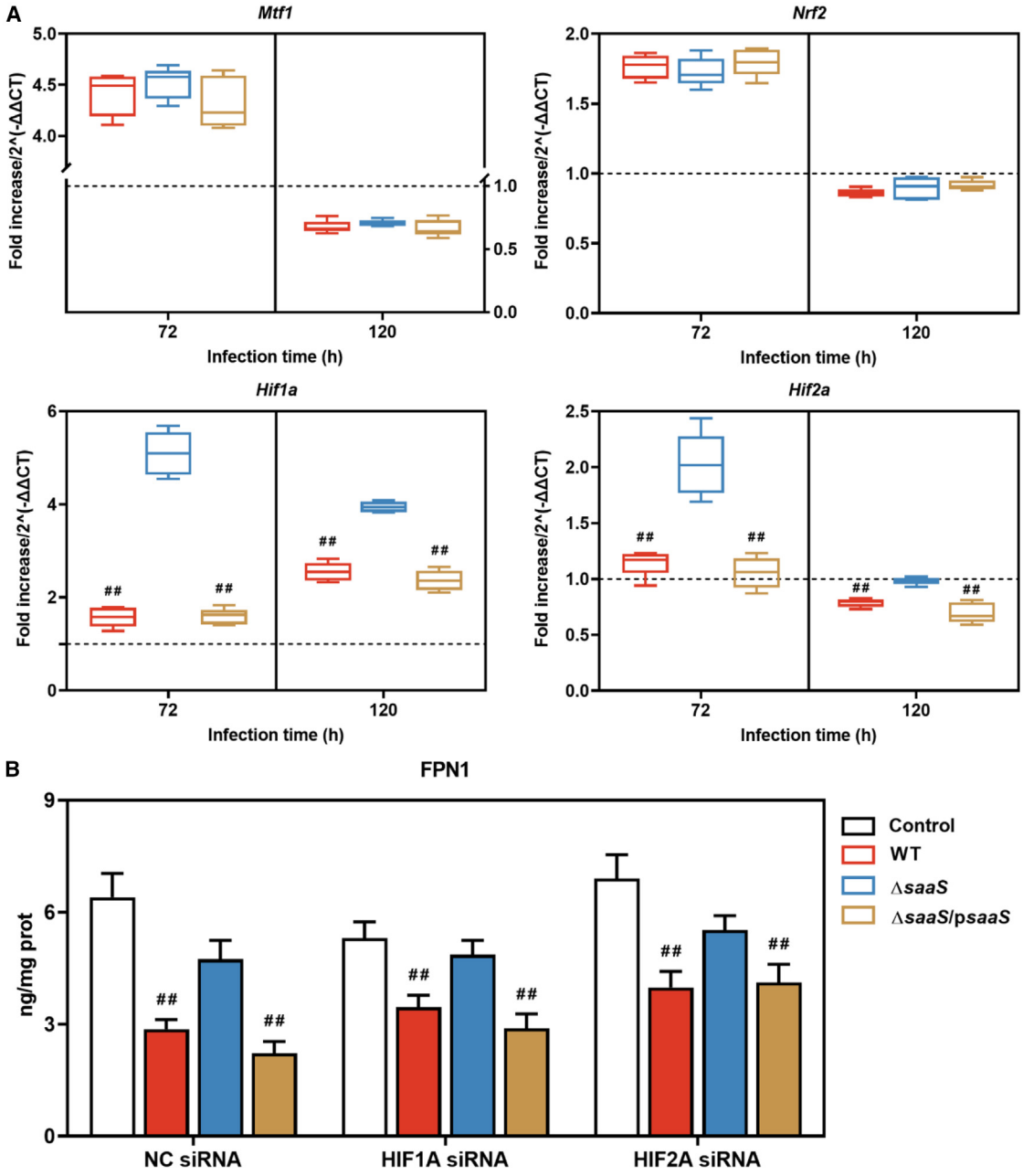

Figure 6. SaaS decreases hepatic FPN1 level by inhibiting *Hif2a* expression

(A) The gene expressions of *Mtf1* (encoding metal regulatory transcription factor 1), *Nrf2* (encoding nuclear factor erythroid-2-related factor 2), *Hif1a* (encoding hypoxia-inducible factor 1α), and *Hif2a* (encoding hypoxia-inducible factor 2α) after indicated infection length, $N = 8$.

(B) The concentration of ferroportin 1 (FPN1) in HepG2 cells infected with *Salmonella* after transfection with the corresponding small interfering RNA (siRNA), $n = 5$. For RT-qPCR analysis, the dash line was corresponding to the control group.

Data are represented as mean ± SD. Statistical significance was determined by an independent Student's t test. $^{*}p < 0.05$, $^{**}p < 0.01$ versus control; $^{\#}p < 0.05$, $^{\#\#}p < 0.01$ versus Δ*saaS*.

ERRγ is also indispensable in the JAK/STAT3 pathway-mediated hepcidin production. Hepatic ERRγ expression, regulated by IL-6-mediated transactivation of STAT3, can induce hepcidin production and lead to eventual hypoferremia in mice. Furthermore, the ablation of *Esrrg* mRNA in the liver can normalize these responses.[29] In this study, despite the successful activation of TREM1, IL-6, and pSTAT3, the effect was gradually attenuated and insufficient to further promote the expression of *Esrrg* mRNA, resulting in undifferentiated *Esrrg* mRNA expression and, ultimately, no impact on hepcidin production. Nevertheless,

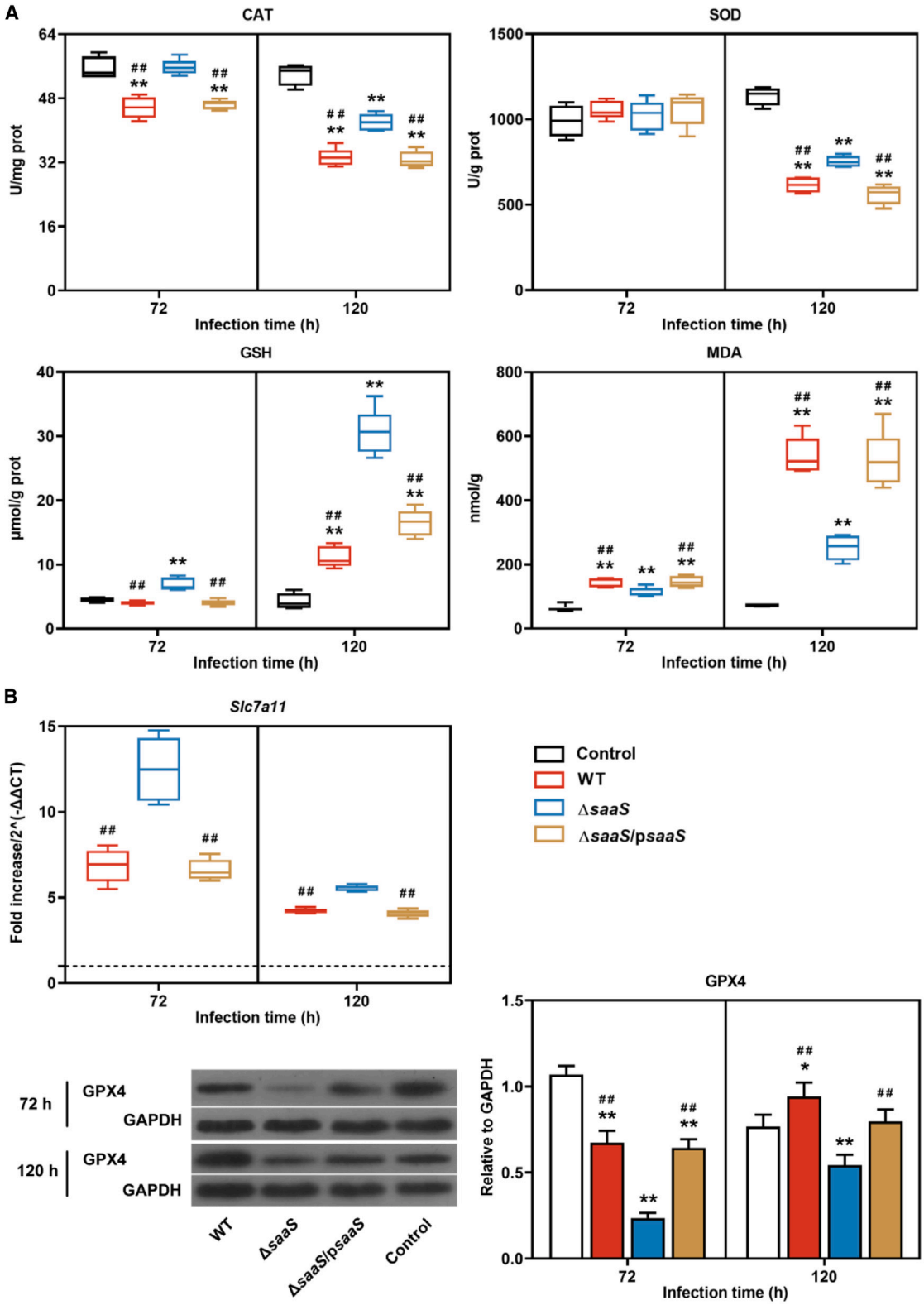

(legend on next page)

this study successfully correlated the activated JAK/STAT pathway with the pro-inflammatory response in the liver. Almost all liver diseases are accompanied by inflammation,[38] and continuous inflammatory stimuli typically contribute to significant damage to hepatic cells and liver function.[39] The aforementioned TREM1 is upregulated during bacterial infections and has been shown to significantly exacerbate hepatic inflammation.[18,40] In line with the elevated IL-6 levels, the expression of *Trem1* mRNA and various pro-inflammatory cytokines was enhanced, while the levels of anti-inflammatory cytokines were diminished. This indicates a cascading amplification of the hepatic inflammatory response via the SaaS-mediated JAK/STAT pathway.

In comparison to hepcidin, *Hif2a* takes precedence in regulating FPN1 at the transcriptional level. The HIF family modulates the expression of iron-associated factors, such as DMT1 and DcytB, during acute iron deficiency,[41] which is crucial for iron metabolism and cellular survival. Beyond its role in iron homeostasis, HIF2A serves as the principal regulator of erythropoiesis; mutations in HIF2A lead to dysregulation of erythropoiesis,[42] which aligns with the observed decrease in RBCs in this study. While the relationships between SaaS and the HIF family were explored here, the reason why the downregulation observed at the mRNA level is not reflected at the functional (protein) level remains unclear.

Excess iron can generate hydroxyl-free radicals through the Fenton reaction, leading to liver impairment via oxidative stress.[43,44] Increased levels of MDA and decreased activities of antioxidant enzymes, such as SOD, CAT, and GSH, typically indicate the presence of oxidative stress and subsequent cellular injury.[44,45] As anticipated, SaaS-induced oxidative stress was confirmed by the reduction in the activities of these antioxidant enzymes and the elevation of MDA levels. To mitigate oxidative stress in the liver, CP is synthesized to catalyze the conversion of Fe^{2+} to Fe^{3+}, with ferritin released to transport, and store excess free iron in the liver.[46,47] Interestingly, SaaS was observed to suppress the levels of CP and ferritin, potentially contributing to the heightened oxidative stress observed in this study. Furthermore, increased bacterial colonization results in greater secretion of lipopolysaccharides by gram-negative bacteria, such as *Salmonella*, which can trigger downstream signaling cascades that elevate oxidative stress, promote cell death, and even lead to ferroptosis. Despite the presence of critical prerequisites, including iron overload and oxidative stress, ferroptosis was not induced by SaaS, likely due to the upregulation of GPX4 protein levels, a key regulator of ferroptosis. The impaired xCT system, consisting of SLC3A2 and SLC7A11, partially accounts for the reduced GSH levels observed with SaaS, as it is responsible for importing cysteine necessary for GSH biosynthesis.[48]

In summary, this study proved that SaaS sRNA is essential for *Salmonella*-induced dysregulation of host iron homeostasis. Focusing on FPN1, SaaS activates the HJV-mediated BMP/SMAD pathway, leading to the upregulation of hepatic hepcidin, which degrades FPN1 and results in hepatic iron accumulation and hypoferremia. SaaS sRNA contributes to the activation of the TREM1-mediated IL-6/JAK/STAT3 pathway, which enhances hepatic inflammatory levels rather than promoting hepcidin expression. Furthermore, the iron accumulation mediated by SaaS promotes a hepatic oxidative response. This study advances our understanding of the pathogenicity associated with the sRNA SaaS in *Salmonella*.

Bacterial pathogens have evolved virulence factors to colonize, replicate, and disseminate within the host. sRNAs have been known as critical virulence factors and regulators in the virulence of pathogens, especially that of the *Salmonella*, but how sRNAs regulate the behavior of pathogens within the host is unknown. In the absence or complement of sequence to sRNAs of interest, investigating the function of sRNAs can be achieved *in vivo*. Here, we validated sRNA SaaS-mediated FPN1 suppression as an effective strategy for *Salmonella* to antagonize nutritional immunity, namely iron competition, in the host and identified the BMP-SMAD pathway as the critical manner. Meanwhile, the SaaS-mediated regulation triggered iron accumulation in the liver and led to hepatic oxidative stress. Our data indicate that SaaS also activated the STAT3 pathway in a TREM1-IL-6-dependent manner, intensifying the hepatic inflammatory response. The successful investigation of the function of sRNAs in *Salmonella*-host interaction has significant implications, not only highlighting the essential roles of sRNAs in pathogenicity and guiding researchers to focus on these important regulators for further investigation but also providing a straightforward target for the control of various pathogens.

Limitations of the study

In this study, we found that sRNA SaaS can regulate the hepcidin-FPN1 axis with the HJV indispensable. However, the underlying mechanisms of SaaS regulating HJV in the liver remains unclear, and further experimental studies are needed. In addition, after SaaS-mediated invasion, the different manners of iron uptake by the transferrin and non-transferrin routes will require further elucidation. In studies of pathogen-host interactions, particularly those involving *Salmonella* and its interactions with mice, young female mice are commonly employed as animal models. Given considerations of animal ethics and the appropriateness of using young female mice, this study did not include male mice. However, it is important to note that the physiological cycle of female mice, characterized by relatively unstable

Figure 7. SaaS triggers oxidative stress in the liver

(A) The concentration of hepatic catalase (CAT), superoxide dismutase (SOD), glutathione (GSH), and malondialdehyde (MDA) after indicated infection length, $N = 8$.

(B) The gene expression of hepatic *Slc7a11* (encoding solute carrier family 11, member 1) and western blot analysis of liver lysates with specific antibodies to GPX4 after indicated infection length. For RT-qPCR analysis, the dash line was corresponding to the control group. For western blot analysis, densitometric analysis of GPX4 protein to GAPDH protein is shown.

Data are represented as mean ± SD. Statistical significance was determined by an independent Student's t test. $^{*}p < 0.05$, $^{**}p < 0.01$ versus control; $^{\#}p < 0.05$, $^{\#\#}p < 0.01$ versus Δ*saaS*.

hormones and other bodily substances, may affect the generalizability of the findings.

RESOURCE AVAILABILITY

Lead contact

Further information and requests for resources and reagents should be directed to and will be fulfilled by the lead contact, Huhu Wang (huuwang@njau.edu.cn).

Materials availability

This study did not generate new unique reagents.

Data and code availability

- All data are available within the paper or supplemental information.
- This paper does not report original code.
- Any additional information required to reanalyze the data reported in this paper is available from the lead contact upon request.

ACKNOWLEDGMENTS

We thank the National Center of Meat Quality and Safety Control and the Joint International Research Laboratory of Animal Health and Food Safety for providing an excellent platform. This work was supported by the National Natural Science Foundation of China (31872911), Youth Project of National Natural Science Foundation of Jiangsu Province (BK20241570), the China Postdoctoral Science Foundation (2024M751432), the Postdoctoral Fellowship Program of CPSF (GZB20240315), Jiangsu Funding Program for Excellent Postdoctoral Talent (2024ZB819), and Priority Academic Program Development of Jiangsu Higher Education Institutions (PAPD).

AUTHOR CONTRIBUTIONS

Conceptualization, L.C., X.X., and H.W.; methodology, L.C., Y.X., and L.S.; investigation, L.C., C.L., and H.H.; supervision, H.W., X.X., and G.Z.; writing – original draft, L.C., Y.X., H.H., C.L., L.S., and H.W.; writing – review and editing, L.C., H.W., and X.X. All the authors discussed the whole paper.

DECLARATION OF INTERESTS

The authors declare no competing interests.

STAR★METHODS

Detailed methods are provided in the online version of this paper and include the following:

- KEY RESOURCES TABLE
- EXPERIMENTAL MODEL AND STUDY PARTICIPANT DETAILS
  - Animals
  - *Salmonella* strains
  - Cell culture and reagents
  - *Salmonella* infection model
- METHOD DETAILS
  - Biomarkers and iron parameters
  - Correlation analysis
  - Quantitative real-time PCR (RT-qPCR)
  - Western blotting
  - Histopathological examination
  - Transient transfection assay
  - Oxidative stress assay
- QUANTIFICATION AND STATISTICAL ANALYSIS

SUPPLEMENTAL INFORMATION

Supplemental information can be found online at https://doi.org/10.1016/j.isci.2024.111660.

Received: May 3, 2024
Revised: September 22, 2024
Accepted: December 18, 2024
Published: December 20, 2024

REFERENCES

1. Eguale, T., Gebreyes, W.A., Asrat, D., Alemayehu, H., Gunn, J.S., and Engidawork, E. (2015). Non-typhoidal *Salmonella* serotypes, antimicrobial resistance and co-infection with parasites among patients with diarrhea and other gastrointestinal complaints in Addis Ababa, Ethiopia. BMC Infect. Dis. *15*, 497–511. https://doi.org/10.1186/s12879-015-1235-y.
2. Sanchez-Vargas, F.M., Abu-El-Haija, M.A., and Gomez-Duarte, O.G. (2011). *Salmonella* infections: an update on epidemiology, management, and prevention. Trav. Med. Infect. Dis. *9*, 263–277. https://doi.org/10.1016/j.tmaid.2011.11.001.
3. Saha, P., Xiao, X., Yeoh, B.S., Chen, Q., Katkere, B., Kirimanjeswara, G.S., and Vijay-Kumar, M. (2019). The bacterial siderophore enterobactin confers survival advantage to *Salmonella* in macrophages. Gut Microb. *10*, 412–423. https://doi.org/10.1080/19490976.2018.1546519.
4. Kirk, M.D., Pires, S.M., Black, R.E., Caipo, M., Crump, J.A., Devleesschauwer, B., Döpfer, D., Fazil, A., Fischer-Walker, C.L., Hald, T., et al. (2015). World health organization estimates of the global and regional disease burden of 22 foodborne bacterial, protozoal, and viral diseases, 2010: A data synthesis. PLoS Med. *12*, e1001921. https://doi.org/10.1371/journal.pmed.1001921.
5. CDC (2019). Surveillance for Foodborne Disease Outbreaks, United States, 2017, Annual Report (Atlanta, Georgia: U.S. Department of Health and Human Services).
6. European Food Safety Authority; European Centre for Disease Prevention and Control (2022). The European Union one health 2021 zoonoses report. EFSA J. *20*, e07666. https://doi.org/10.2903/j.efsa.2022.7666.
7. Hood, M.I., and Skaar, E.P. (2012). Nutritional immunity: Transition metals at the pathogen-host interface. Nat. Rev. Microbiol. *10*, 525–537. https://doi.org/10.1038/nrmicro2836.
8. Andreini, C., Bertini, I., Cavallaro, G., Holliday, G.L., and Thornton, J.M. (2008). Metal ions in biological catalysis: From enzyme databases to general principles. J. Biol. Inorg. Chem. *13*, 1205–1218. https://doi.org/10.1007/s00775-008-0404-5.
9. Nairz, M., and Weiss, G. (2020). Iron in infection and immunity. Mol. Aspect. Med. *75*, 100864. https://doi.org/10.1016/j.mam.2020.100864.
10. Núñez, G., Sakamoto, K., and Soares, M.P. (2018). Innate nutritional immunity. J. Immunol. *201*, 11–18. https://doi.org/10.4049/jimmunol.1800325.
11. Jia, H., Song, N., Ma, Y., Zhang, F., Yue, Y., Wang, W., Li, C., Li, H., Wang, Q., Gu, L., and Li, B. (2022). *Salmonella* facilitates iron acquisition through umpylation of ferric uptake regulator. mBio *13*, e0020722. https://doi.org/10.1128/mbio.00207-22.
12. Kim, J.N. (2016). Roles of two RyhB paralogs in the physiology of *Salmonella enterica*. Microbiol. Res. *186–187*, 146–152. https://doi.org/10.1016/j.micres.2016.04.004.
13. Hébrard, M., Kröger, C., Srikumar, S., Colgan, A., Händler, K., and Hinton, J.C.D. (2012). sRNAs and the virulence of *Salmonella enterica* Serovar Typhimurium. RNA Biol. *9*, 437–445. https://doi.org/10.4161/rna.20480.
14. Dong, R., Liang, Y., He, S., Cui, Y., Shi, C., He, Y., and Shi, X. (2022). DsrA modulates central carbon metabolism and redox balance by directly repressing *pflB* expression in *Salmonella* Typhimurium. Microbiol. Spectr. *10*, e0152221. https://doi.org/10.1128/spectrum.01522-21.

15. Nicole, R., Disha, T., Siegfried, H., and Polacek, N. (2022). The stationary phase-specific sRNA FimR2 is a multifunctional regulator of bacterial motility, biofilm formation and virulence. Nucleic Acids Res. *20*, 50–63. https://doi.org/10.1093/nar/gkac1025.

16. Wang, C.Y., and Babitt, J.L. (2019). Liver iron sensing and body iron homeostasis. Blood *133*, 18–29. https://doi.org/10.1182/blood-2018-06-815894.

17. Ganz, T. (2019). The discovery of the iron-regulatory hormone hepcidin. Clin. Chem. *65*, 1330–1331. https://doi.org/10.1373/clinchem.2019.306407.

18. Deng, Q., Yang, S., Sun, L., Dong, K., Li, Y., Wu, S., and Huang, R. (2021). *Salmonella* effector SpvB aggravates dysregulation of systemic iron metabolism via modulating the hepcidin-ferroportin axis. Gut Microb. *13*, 1–18. https://doi.org/10.1080/19490976.2020.1849996.

19. Jia, K., Wang, H.H., Xu, X.L., Zhou, G.H., and He, S.W. (2020). Novel sRNA and regulatory genes repressing the adhesion of *Salmonella* Enteritidis exposed to meat-related environment. Food Control *110*, 107030. https://doi.org/10.1016/j.foodcont.2019.107030.

20. Cai, L.L., Xie, Y.T., Hu, H.J., Xu, X.L., Wang, H.H., and Zhou, G.H. (2023). A small RNA, SaaS, promotes *Salmonella* pathogenicity by regulating invasion, intracellular growth, and virulence factors. Microbiol. Spectr. *11*, e0293822. https://doi.org/10.1128/spectrum.02938-22.

21. Moreira, A.C., Neves, J.V., Silva, T., Oliveira, P., Gomes, M.S., and Rodrigues, P.N. (2017). Hepcidin-(in) dependent mechanisms of iron metabolism regulation during infection by *Listeria* and *Salmonella*. Infect. Immun. *85*, e00353-17. https://doi.org/10.1128/IAI.00353-17.

22. Schwartz, A.J., Das, N.K., Ramakrishnan, S.K., Jain, C., Jurkovic, M.T., Wu, J., Nemeth, E., Lakhal-Littleton, S., Colacino, J.A., and Shah, Y.M. (2019). Hepatic hepcidin/intestinal HIF-2α axis maintains iron absorption during iron deficiency and overload. J. Clin. Invest. *129*, 336–348. https://doi.org/10.1172/JCI122359.

23. Dore, M.P., Tomassini, G., Rocchi, C., Bulajic, M., Carta, M., Errigo, A., Dimaggio, A., Padedda, F., and Pes, G.M. (2023). Risk of hemolytic anemia in IBD patients with glucose-6-phosphate dehydrogenase deficiency treated with mesalamine: Results of a retrospective-prospective and *ex vivo* study. J. Clin. Med. *12*, 4797. https://doi.org/10.3390/jcm12144797.

24. Camaschella, C., Nai, A., and Silvestri, L. (2020). Iron metabolism and iron disorders revisited in the hepcidin era. Haematologica *105*, 260–272. https://doi.org/10.3324/haematol.2019.232124.

25. Rochette, L., Gudjoncik, A., Guenancia, C., Zeller, M., Cottin, Y., and Vergely, C. (2015). The iron-regulatory hormone hepcidin: A possible therapeutic target? Pharmacol. Ther. *146*, 35–52. https://doi.org/10.1016/j.pharmthera.2014.09.004.

26. Besson-Fournier, C., Latour, C., Gourbeyre, O., Aguilar-Martinez, P., Silvestri, L., Roth, M.P., and Coppin, H. (2014). Transferrin receptor 2 and HFE regulate hepcidin levels independently of BMP6 and hemojuvelin. Blood *124*, 746–758. https://doi.org/10.1182/blood.V124.21.746.746.

27. Silvestri, L., Guillem, F., Pagani, A., Nai, A., Oudin, C., Silva, M., Toutain, F., Kannengiesser, C., Beaumont, C., Camaschella, C., and Grandchamp, B. (2009). Molecular mechanisms of the defective hepcidin inhibition in TMPRSS6 mutations associated with iron-refractory iron deficiency anemia. Blood *113*, 5605–5608. https://doi.org/10.1182/blood-2008-12-195594.

28. Kim, D.K., Jeong, J.H., Lee, J.M., Kim, K.S., Park, S.H., Kim, Y.D., Koh, M., Shin, M., Jung, Y.S., Kim, H.S., et al. (2014). Inverse agonist of estrogen-related receptor gamma controls *Salmonella* Typhimurium infection by modulating host iron homeostasis. Nat. Med. *20*, 419–424. https://doi.org/10.1038/nm.3483.

29. Yang, S., Deng, Q., Sun, L., Dong, K., Li, Y., Wu, S., and Huang, R. (2019). *Salmonella* effector SpvB interferes with intracellular iron homeostasis via regulation of transcription factor NRF2. Faseb. J. *33*, 13450–13464. https://doi.org/10.1096/fj.201900883RR.

30. Stockwell, B.R., Friedmann Angeli, J.P., Bayir, H., Bush, A.I., Conrad, M., Dixon, S.J., Fulda, S., Gascón, S., Hatzios, S.K., Kagan, V.E., et al. (2017). Ferroptosis: A regulated cell death nexus linking metabolism, redox biology, and disease. Cell *171*, 273–285. https://doi.org/10.1016/j.cell.2017.09.021.

31. Zou, Y., Palte, M.J., Deik, A.A., Li, H., Eaton, J.K., Wang, W., Tseng, Y.Y., Deasy, R., Kost-Alimova, M., Dančík, V., et al. (2019). A GPX4-dependent cancer cell state underlies the clear-cell morphology and confers sensitivity to ferroptosis. Nat. Commun. *10*, 1617–1630. https://doi.org/10.1038/s41467-019-09277-9.

32. Ginzburg, Y.Z., Feola, M., Zimran, E., Varkonyi, J., Ganz, T., and Hoffman, R. (2018). Dysregulated iron metabolism in polycythemia vera: etiology and consequences. Leukemia *32*, 2105–2116. https://doi.org/10.1038/s41375-018-0207-9.

33. Zhang, D.L., Wu, J., Shah, B.N., Greutélaers, K.C., Ghosh, M.C., Ollivierre, H., Su, X.Z., Thuma, P.E., Bedu-Addo, G., Mockenhaupt, F.P., et al. (2018). Erythrocytic ferroportin reduces intracellular iron accumulation, hemolysis, and malaria risk. Science *359*, 1520–1523. https://doi.org/10.1126/science.aal2022.

34. Zheng, J., and Conrad, M. (2020). The metabolic underpinnings of ferroptosis. Cell Metabol. *32*, 920–937. https://doi.org/10.1016/j.cmet.2020.10.011.

35. Chen, P.H., Wu, J., Ding, C.K.C., Lin, C.C., Pan, S., Bossa, N., Xu, Y., Yang, W.H., Mathey-Prevot, B., and Chi, J.T. (2020). Kinome screen of ferroptosis reveals a novel role of ATM in regulating iron metabolism. Cell Death Differ. *27*, 1008–1022. https://doi.org/10.1038/s41418-019-0393-7.

36. Shang, Y., Luo, M., Yao, F., Wang, S., Yuan, Z., and Yang, Y. (2020). Ceruloplasmin suppresses ferroptosis by regulating iron homeostasis in hepatocellular carcinoma cells. Cell. Signal. *72*, 109633. https://doi.org/10.1016/j.cellsig.2020.109633.

37. Babitt, J.L., and Lin, H.Y. (2010). Molecular mechanisms of hepcidin regulation: Implications for the anemia of CKD. Am. J. Kidney Dis. *55*, 726–741. https://doi.org/10.1053/j.ajkd.2009.12.030.

38. Han, C., Wu, X., Zou, N., Zhang, Y., Yuan, J., Gao, Y., Chen, W., Yao, J., Li, C., Hou, J., and Qin, D. (2021). *Cichorium pumilum* jacq extract inhibits LPS-induced inflammation via MAPK signaling pathway and protects rats from hepatic fibrosis caused by abnormalities in the gut-liver axis. Front. Pharmacol. *12*, 683613. https://doi.org/10.3389/fphar.2021.683613.

39. Wu, M., Wang, C., Mai, C., Chen, J., Lai, X., He, L., Huang, S., and Zhang, X. (2019). Flavonoids from *Livistona chinensis* fruit ameliorates LPS/D-GalN-induced acute liver injury by inhibiting oxidative stress and inflammation. J. Funct.Foods *61*, 103460. https://doi.org/10.1016/j.jff.2019.103460.

40. Han, L., Fu, L., Peng, Y., and Zhang, A. (2018). Triggering receptor expressed on myeloid cells-1 signaling: Protective and pathogenic roles on streptococcal toxic-shock-like syndrome caused by *Streptococcus suis*. Front. Immunol. *9*, 577–597. https://doi.org/10.3389/fimmu.2018.00577.

41. Shah, Y.M., Matsubara, T., Ito, S., Yim, S.H., and Gonzalez, F.J. (2009). Intestinal hypoxia-inducible transcription factors are essential for iron absorption following iron deficiency. Cell Metabol. *9*, 152–164. https://doi.org/10.1016/j.cmet.2008.12.012.

42. Ghosh, M.C., Zhang, D.L., Jeong, S.Y., Kovtunovych, G., Ollivierre-Wilson, H., Noguchi, A., Tu, T., Senecal, T., Robinson, G., Crooks, D.R., et al. (2013). Deletion of iron regulatory protein 1 causes polycythemia and pulmonary hypertension in mice through translational derepression of HIF2 alpha. Cell Metabol. *17*, 271–281. https://doi.org/10.1016/j.cmet.2012.12.016.

43. Sinha, S., Pereira-Reis, J., Guerra, A., Rivella, S., and Duarte, D. (2021). The role of iron in benign and malignant hematopoiesis. Antioxidants Redox Signal. *35*, 415–432. https://doi.org/10.1089/ars.2020.8155.

44. Cui, J., Zhou, Q., Yu, M., Liu, Y., Teng, X., and Gu, X. (2022). 4-tert-butylphenol triggers common carp hepatocytes ferroptosis via oxidative stress,

iron overload, SLC7A11/GSH/GPX4 axis, and ATF4/HSPA5/GPX4 axis. Ecotoxicol. Environ. Saf. *242*, 113944. https://doi.org/10.1016/j.ecoenv.2022.113944.

45. Shi, X., Li, X.J., Sun, X.Y., Cui, W., and Liu, H.G. (2021). Pig lung fibrosis is active in the subacute $CdCl_2$ exposure model and exerts cumulative toxicity through the M1/M2 imbalance. Ecotoxicol. Environ. Saf. *225*, 112757. https://doi.org/10.1016/j.ecoenv.2021.112757.
46. Protchenko, O., Baratz, E., Jadhav, S., Li, F., Shakoury-Elizeh, M., Gavrilova, O., Ghosh, M.C., Cox, J.E., Maschek, J.A., Tyurin, V.A., et al. (2021). Iron chaperone poly rC binding protein 1 protects mouse liver from lipid peroxidation and steatosis. Hepatology *73*, 1176–1193. https://doi.org/10.1002/hep.31328.
47. Corradini, E., Buzzetti, E., Dongiovanni, P., Scarlini, S., Caleffi, A., Pelusi, S., Bernardis, I., Ventura, P., Rametta, R., Tenedini, E., et al. (2021). Ceruloplasmin gene variants are associated with hyperferritinemia and increased liver iron in patients with NAFLD. J. Hepatol. *75*, 506–513. https://doi.org/10.1016/j.jhep.2021.03.014.
48. Koppula, P., Zhuang, L., and Gan, B. (2021). Cystine transporter SLC7A11/xCT in cancer: Ferroptosis, nutrient dependency, and cancer therapy. Protein Cell *12*, 599–620. https://doi.org/10.1007/s13238-020-00789-5.
49. Wang, H., Cai, L., Hu, H., Xu, X., and Zhou, G. (2019). Complete genome sequence of *Salmonella enterica* Serovar Enteritidis NCM 61, with high potential for biofilm formation, isolated from meat-related sources. Microbiol. Resour. Announc. *8*, 10–1128. https://doi.org/10.1128/MRA.01434-18.
50. Li, X., Shan, K., Li, C., and Zhou, G. (2023). Intermittent protein diets alter hepatic lipid accumulation by changing tryptophan metabolism in a fast-response manner. J. Agric. Food Chem. *71*, 3261–3272. https://doi.org/10.1021/acs.jafc.2c06576.
51. Wu, Z., Zhang, W., Zhao, X., and Xu, X. (2024). Gastrointestinal digestion behavior and bioavailability of greenly prepared highly loaded myofibrillar-luteolin vehicle. Food Res. Int. *187*, 114413. https://doi.org/10.1016/j.foodres.2024.114413.
52. Cai, L.L., Xie, Y.T., Hu, H.J., Xu, X.L., Wang, H.H., and Zhou, G.H. (2024). Multi-omics approaches reveal inflammatory response and intestinal damage mediated by sRNA SaaS during *Salmonella* invasion in mice. Food Front. *5*, 1749–1764. https://doi.org/10.1002/fft2.421.
53. Cai, L., Xie, Y., Shao, L., Hu, H., Xu, X., Wang, H., and Zhou, G. (2023). SaaS sRNA promotes *Salmonella* intestinal invasion via modulating MAPK inflammatory pathway. Gut Microb. *15*, 2211184. https://doi.org/10.1080/19490976.2023.2211184.

STAR★METHODS

KEY RESOURCES TABLE

REAGENT or RESOURCE	SOURCE	IDENTIFIER
Antibodies		
Phospho-Smad1(Ser463/465)/Smad5 (Ser463/465)/Smad9 (Ser465/467)	Cell Signaling Technology	Cat#13820; RRID:AB_2493181
Phospho-STAT3 (Tyr705)	Abcam	Cat#ab32143; RRID:AB_2286742
GPX4	Abcam	Cat#ab125066; RRID:AB_10973901
GAPDH	Thermo Pierce	Cat#ab9485; RRID:AB_307275
Goat anti-Mouse IgG (H + L) Secondary antibody	Thermo Pierce	Cat#31210; RRID:AB_228334
Bacterial and virus strains		
Salmonella Enteritidis: WT	Isolated from contact surfaces of meat processing equipment (Wang et al.[49])	NCM61
Salmonella Enteritidis: Δ*saaS*	Deleting *saaS* gene based on WT (Wang et al.[49])	NCM282
Salmonella Enteritidis: Δ*saaS*/p*saaS*	Completing *saaS* gene based on Δ*saaS*/p*saaS* (Wang et al.[49])	N/A
Chemicals, peptides, and recombinant proteins		
Luria-Bertani broth	HopeBio	HB0128
DMEM	HyClone	SH30022.01B
Hieff Trans™ *in vitro* siRNA/miRNA Transfection Reagent	Yeasen	40806ES02
Cell lysis buffer for Western and IP	Beyotime	P0013
PrimeScript™ RT Master Mix	Takara	RR036
ChamQ Universal SYBR qPCR Master Mix	Vazyme	Q711
Critical commercial assays		
FastPure Cell/Tissue Total RNA Isolation Kit	Vazyme	RC101
BCA protein assay kit	Thermo Scientific	23225
Mouse Ferroportin1 (FPN1) ELISA Kit	Ruidahenghui	RD-RX28086
Total Superoxide Dismutase Assay Kit with WST-8	Beyotime	S0101S
Experimental models: Cell lines		
Human: HepG2 cells	Cell Bank of the Chinese Academy of Sciences	SCSP-510
Experimental models: Organisms/strains		
Mouse: BALB/c	Ziyuan Laboratory Animal Technology Company	N/A
Oligonucleotides		
Primers for strain construction, see Table S1	This paper	N/A
Primers for RT-qPCR analysis and sequences of siRNA duplexes, see Table S2	This paper	N/A
Recombinant DNA		
Plasmids for strain construction, See Table S1	This paper	N/A
Software and algorithms		
ImageJ	National Institutes of Health, USA	https://imagej.nih.gov/ij/
SAS	SAS Institute Inc	https://www.sas.com
Prism	GraphPad	https://www.graphpad.com/scientificsoftware/prism/

EXPERIMENTAL MODEL AND STUDY PARTICIPANT DETAILS

Animals

Six to seven-week-old female BALB/c mice (Specified pathogen-free, SPF) were provided by Ziyuan Laboratory Animal Technology Company (Wuhan, China). These mice were placed under SPF controlled environment (SYXK<Hubei>2018-0069; 12 h cycle of light, 23.0 ± 0.5°C of temperature and 60 ± 10% of humidity). All experiments involving animals were conducted according to the ethical policies and procedures of the Ethical Committee of the Experimental Animal Center of Nanjing Agricultural University and the Ethical Committee of Wuhan cloud-clone Technology company (Approval no. IACU21-0813).

Salmonella strains

S. Enteritidis strain (Reference genome GenBank: CP032851.1) used in this study was isolated from contact surfaces of meat processing equipment.[49] This original strain was set as WT. The generation of Δ*saaS* and Δ*saaS*/p*saaS* was briefly described as follows.[20] For the *saaS* deletion mutant, the allelic exchange using the suicide plasmid was used. The upstream and downstream homologous recombination arms of the *saaS* gene from the WT genome and the kanamycin resistance (Knr) gene from the pKD4 plasmid were amplified using the primer pairs *saaS*-5F/5R, *saaS*-3F/3R, and Kn-F/R, respectively (Table S1). The three sequences were bridged by fusion PCR to obtain the complete target fragment Δ*saaS*::Kn (upstream homologous arm-Knr gene-downstream homologous arm), and Δ*saaS*::Kn was then cloned into the general vector pUC19 to obtain the intermediate plasmid pUC19-Δ*saaS*::Kn. Second, the target fragment Δ*saaS*::Kn was subcloned into the suicide plasmid pCVD442 following confirmation by sequencing with the above intermediate plasmid to obtain pCVD442-Δ*saaS*::Kn. The donor strain β2155/pCVD442-Δ*saaS*::Kn was obtained by transferring pCVD442-ΔsaaS::Kn into *Escherichia* coli β2155. The donor strain and the recipient strain WT were conjugated, and the *Salmonella* clones obtaining Knr were collected and named Sen/pCVD442-Δ*saaS*::Kn. Ultimately, knockout mutants (Δ*saaS*) were produced by electroporating plasmid pCP20 into the competent cells of Sen/pCVD442-Δ*saaS*::Kn and named *S*. Enteritidis strain NCM282.

The *saaS* gene and the low-copy-number pRK415 expression vector were amplified for the complemented strain using primers *saaS*-F/R and pRK415-F/R, respectively. Following gel purification and HindIII/EcoRI digestion, the digested *saaS* and pRK415 products were ligated for 2 h at 37°C to generate the constructed plasmid pRK415-*saaS*. pRK415-*saaS* was subsequently transferred into the mutant Δ*saaS* strain and selected on tetracycline (Tc; 10 mg/mL) plates to yield the complemented strain (Δ*saaS*/p*saaS*). Three strains were cultured overnight in Luria-Bertani broth (LB; HopeBiotechnology, Beijing, China) at 37°C before use.

Cell culture and reagents

The HepG2 cells (human hepatoma cells) used in our study were obtained from the Cell Bank of the Chinese Academy of Sciences (Shanghai, China). *HJV* siRNA, *TMPRSS6* siRNA, *HIF1A* siRNA, *HIF2A* siRNA, and negative control (NC) siRNA were produced by GenePharma company (Shanghai, China). These siRNAs were used to treat cells for the gene silencing, and the sequences were shown in Table S2. The HepG2 cells have not been authenticated or tested for mycoplasma contamination. Nevertheless, this cell line has consistently been passaged in our cell laboratory, and the corresponding research has been widely recognized,[50,51] which could indirectly confirm the reliability of this cell line.

Salmonella infection model

Before infection, *Salmonella* strains WT, Δ*saaS* and Δ*saaS*/p*saaS* were washed, resuspended, and diluted with 0.85% NaCl solution to a concentration of 10^9 CFU/mL. After 4-h fast, mice were infected with 1×10^8 colony-forming units (CFU) *S*. Enteritidis strains in 100 μL of PBS as treatment group or 100 μL PBS as control group by oral gavage. In the previous study,[20] the significant differences in both of the weight and food intake between the Δ*saaS* strain-infected group and WT strain-infected group or Δ*saaS*/p*saaS* strain-infected group were first discovered at the 72-h post infection (hpi). Hence, we choose 72 hpi as the first key observation point. Meanwhile, the death of the mice was successively occurred from 144 hpi (6^{th} day), suggesting that the physiology of mice was gradually damaged. Hence, we choose 120 hpi as the final key observation point. At 72 and 120 hpi, the liver and blood of each mouse were collected with sterile tools and stored in sterile tubes for the next experiments.

METHOD DETAILS

Biomarkers and iron parameters

Hemogram parameters, including RBC, HGB, HCT, MCV, MCH, MCHC, and RDW-CV, were determined with anticoagulation whole blood using an auto-hematology analyzer (BC2800Vet; Mindray, Shenzhen, China). Liver function parameters, including serum AST, ALT, and LDH levels, were determined as per the manufacturer's instructions (Jiancheng, Nanjing, China). Hepatic IL-6 levels were measured using an enzyme-linked immunosorbent assay (ELISA; Angle gene, Nanjing, China). Serum ferritin, UIBC, TIBC and hepatic FPN1 levels were measured by ELISA (Ruidahenghui, Beijing, China). Serum iron content was measured using an iron assay kit (Boxbio, Beijing, China). Serum Tf sat was calculated as the value of serum iron content/TIBC. Hepatic iron content was determined using an iron assay kit (BioAssay Systems, CA, USA). The final content of hepatic FPN1 and iron levels was calculated by dividing each content by the hepatic total protein content determined using a BCA protein assay kit (Thermo Scientific, MA, USA).

Correlation analysis

Previous study has evaluated the bacterial burden in the liver of mice that infected by *Salmonella*.[20] To construct the relationships between bacterial burden and the above plasma and cellular iron status in this study, Spearman's correlation coefficients were evaluated according to previously described method.[52,53] Only significantly different indicators between groups were selected here. For the comparison between two random indicators, the data from four groups in each indicator was utilized. Correlations with |Spearman's rank correlation coefficient| > 0.5 and $p < 0.05$ were considered significant.

Quantitative real-time PCR (RT-qPCR)

Total RNA and cDNA of liver tissues and cells were obtained. qRT-PCR was carried out with a ChamQ Universal SYBR qPCR Master Mix (Vazyme, Nanjing, China) as per the manufacturer's protocols. The specific primer sequences for the target gene were synthesized by GenScript Biotech Corporation and shown in Table S2.

Western blotting

The proteins were extracted using a protein extraction buffer for western blotting and IP (Beyotime, Nantong, China), fractionated by SDS-PAGE and transferred onto PVDF membranes (Millipore, MA, USA). After blocking, the membranes were incubated with antibody (The information was shown in Table S3) for overnight at 4°C. After incubation, membranes were probed with secondary antibody. Finally, target proteins were quantitated via ImageJ (Version 1.53c; NIH, MD, USA).

Histopathological examination

To assess hepatic iron accumulation, Perls' Prussian Blue-DAB staining was carried out as described.[18] Liver samples were fixed in 4% paraformaldehyde and processed using routine histological procedures. Paraffin sections were incubated in the Perls' Prussian blue working solution (Servicebio, Nanjing, China) at 60°C for 30 min and subsequently stained with nuclear fast red at room temperature for 5 min. All representative photomicrographs were captured under a light microscope (BX51; Olympus, Tokyo, Japan).

Transient transfection assay

HepG2 cells were transfected with 15 nM siRNA using Hieff Trans *in vitro* siRNA/miRNA Transfection Reagent siRNA/miRNA (Yeasen, Shanghai, China), according to the manufacturer's instructions. Silencing efficiency was shown in Figure S1. After 24-h transfection, HepG2 cells were infected with WT, Δ*saaS* or Δ*saaS*/p*saaS* at a MOI of 10 for 6 h. Total RNA extraction, reverse transcription, and RT-qPCR were performed as previously described.

Oxidative stress assay

Liver tissue lysates were obtained as described above, and SOD were detected using the Total Superoxide Dismutase Assay Kit with WST-8 (Beyotime, Nantong, China). CAT, GSH, and MDA were detected using commercial kits (Jiancheng, Nanjing, China), according to the manufacturer's instructions. The detection wavelengths were set at 450 nm (SOD), 405 nm (CAT), 405 nm (GSH), and 532 nm (MDA). For SOD, CAT, and GSH, the absorbance value was used to calculate the content of these indices based on total protein levels, while for MDA, the calculation was based on the hepatic weight.

QUANTIFICATION AND STATISTICAL ANALYSIS

Statistical analyses were performed with SAS software (Version 9.2; SAS Institute Inc., NC, USA) and GraphPad Prism (Version 5.0.3; GraphPad Software Inc., CA, USA). Comparisons in this study were conducted between the two groups and analyzed using an independent Student's t test. A p value of less than 0.05 was considered statistically significant. All results are expressed as mean ± standard deviation (SD). Here, n represents the number of cell wells, while N denotes the number of mice, as indicated in the figure legends. Further details regarding the original data and the materials and methods can be found in Datas S1–S7 and Supplemental Material, respectively.